Enhancement of Radiotherapy with Human Mesenchymal Stem Cells Containing Gold Nanoparticles

Mrudula Pullambhatla[1], Steven P. Rowe[1], Ala Lisok[1], Yuchuan Wang[1], Gabriele Putz Todd[2], Alla Danilkovitch[2], and Martin G. Pomper[1]

[1]The Russell H. Morgan Department of Radiology and Radiological Science, Johns Hopkins University School of Medicine, Baltimore, MD; and [2]Osiris Therapeutics, Columbia, MD

Corresponding Author:
Martin G. Pomper, MD, PhD
Johns Hopkins University School of Medicine, 601 N. Caroline Street, Rm 3223, Baltimore, MD, 21217-0014;
E-mail: mpomper@jhmi.edu

Key Words: MSCs, nanomedicine, targeted delivery, breast cancer, tumor microenvironment, molecular imaging

Abbreviations: gold nanoparticle (GNP), mesenchymal stem cell (MSC), human mesenchymal stem cell (hMSC), fetal bovine serum (FBS), phosphate-buffered saline (PBS), nonobese diabetic-severe combined immunodeficiency (NOD-SCID), irradiation (IR), single-photon emission computed tomography (SPECT), computed tomography (CT), small animal radiation research platform (SARRP)

ABSTRACT

Radiotherapy is a common approach for the treatment of a wide variety of cancer types. Available data indicate that nanoparticles can enhance the effect of radiotherapy. We report the use of human mesenchymal stem cells to selectively deliver gold nanoparticles (GNPs) to MDA-MB-231 breast tumor xenografts in mice for the purpose of enhancing the effect of radiation therapy. Targeted delivery of GNPs to the tumor site, followed by irradiation of the tumor, enabled control of tumor growth. The results indicate that tumor-selective GNP delivery by human mesenchymal stem cells may represent a viable way to enhance the effectiveness of radiotherapy.

INTRODUCTION

Radiotherapy is one of the predominant forms of cancer treatment, with 52% of patients with cancer undergoing at least 1 treatment course as either monotherapy or in combination with other therapies (1). In radiotherapy, the tumor is exposed to high-energy radiation (x-rays, γ-rays, charged particles such as electrons or protons) that can destroy proliferative cancer cells through processes that begin by damaging the cancer cells' DNA. Although that mode of therapy is noninvasive, the downside is the damage to the surrounding healthy tissue through the ionizing effects of radiation (2). This limits the dose of radiation that can be safely administered to a given location in a patient.

One way to mitigate this limitation of radiotherapy is by using radiosensitizers—drugs that increase tumor sensitivity to radiotherapy. Multiple chemical radiosensitizers have been developed that target the hypoxic environment within solid tumors, which is considered to play an important role in mediating tumor radioresistance (3–5). Other known chemical radiosensitizers target DNA repair pathways or proteins involved in cell signaling, and can be used in conjunction with radiotherapy to enhance tumor cell killing (6).

Recent advances indicate the potential use of nanoparticles as radiosensitizers and radiotherapy enhancers (7). Based on European Commission recommendations, nanoparticles are particles that range in size from 1 nm to100 nm (8). Gold nanoparticles (GNPs) are among the most widely studied therapeutic nanoparticles, as they are characterized by low systemic toxicity and high cellular uptake. Gold is inert, and the biocompatibility and pharmacokinetics of GNPs can be controlled by choice of coating and functionalization (9, 10). Further, GNPs absorb x-rays, resulting in a dose-enhancement effect (11). The therapeutic effect of GNPs depends on their size, the applied radiation dose, and the tumor type. Large nanoparticles ($\geq$5.5 nm in diameter) have longer blood retention time, but exhibit poor tissue penetration (including within tumors) and demonstrate highest accumulation in liver. In contrast, small nanoparticles ($<$5.5 nm in diameter) are cleared relatively quickly from the body through the kidneys (12, 13).

For successful enhancement of radiotherapy using GNPs, the targeted delivery of nanoparticles to the tumor site is required. Effective tumor targeting can be achieved by attaching tumor-homing moieties to the surface of GNPs. Another option is the targeted delivery of GNPs by cells migrating to the tumor site. Recent evidence suggests that mesenchymal stem cells (MSCs) selectively home to tumors and other sites characterized by the presence of inflammation (14–17). Several studies have shown that developing tumors recruit MSCs by using mechanisms similar to the migration of MSCs to sites of injury and/or inflammation (18–22). That is not surprising, as the microenvironment of a tumor closely resembles the environment of an injured/inflamed tissue, and many of the inflammatory mediators secreted by

ISSN 2379-1381 https://doi.org/10.18383/j.tom.2020.00026

wounds are also found in the tumor microenvironment (19). MSC properties and potential for use as a vehicle for targeted drug delivery are overviewed in detail by Putz Todd et al. (23). The tumor-homing property of MSCs may enable their use as targeted therapeutic delivery vehicles (Figure 1).

The delivery of radiosensitizers to tumor sites by MSCs requires the efficient uptake of GNPs into the carrier cells. The uptake of GNPs with diameters in the range of 14–90 nm has been reported for different cell lines, including MSCs (24–26). Large GNPs were shown to be more easily incorporated into cells than small nanoparticles, with the optimal uptake occurring at 50-nm diameter of spherical GNPs (27, 28). Smaller GNPs exocytose at a faster rate and at a higher percentage than larger ones, which enables faster clearance of the nanoparticles from the body (27).

In the present study, we report enhancement of radiotherapy in mice with MDA-MB-231 cell line–derived breast tumors through targeted delivery of GNPs with human MSCs (hereafter, gold hMSCs) as the carrier. To avoid accumulation of nanoparticles in the liver or spleen, GNPs with a diameter of 1.9 nm (AuroVist™, Nanoprobes Inc., NY) were used. In recent studies AuroVist was shown to be easily cleared from the murine body through the kidneys (29, 30).

METHODOLOGY

Female nonobese diabetic-severe combined immunodeficiency (NOD-SCID) mice were purchased from the National Cancer Institute (Frederick, MD). The human breast cancer cell line MDA-MB-231 was purchased from ATCC (Manassas, VA). Bone marrow hMSCs derived from 1 donor were isolated and cultured as described previously (31). hMSCs at passages 3 and 4 were used for all experiments. All cell culture reagents were purchased from Corning Cell Gro (Manassas, VA) unless specified otherwise. Protamine sulfate salt from salmon was purchased from Sigma-Aldrich (Saint Louis, MO) and AuroVist Gold Nanoparticles (1.9 nm) from Nanoprobes, Inc. (Yaphank, NY).

Preparation of Gold Nanoparticle-Loaded hMSCs

In total, 3 batches of gold hMSCs were prepared. For each batch, expanded hMSCs (passages 3 or 4) were seeded at a density of 30,000 hMSCs/cm^2 and cultured with the Dulbecco modified eagle medium containing 10% fetal bovine serum (FBS; Hyclone, Logan, UT) and 4mM GlutaMAX (Invitrogen, Carlsbad, CA) in a tissue culture incubator (37°C, 5% CO_2). After cells had adhered to the bottom of the tissue culture plastic flasks, the medium was replaced with serum-free medium, and hMSCs were cultured overnight. Following overnight starvation, hMSCs were incubated with AuroVist and protamine sulfate in serum-free medium. The final concentration of protamine sulfate in the culture was 50 μg/μL. Selection of AuroVist concentration depended on results from AuroVist lot qualification testing, which was performed by microscopic analysis of AuroVist nanoparticle adhesion to the hMSC surface in the presence of protamine sulfate and by microscopic evaluation of gold hMSC adhesion to the tissue culture plastic during cell harvesting. The selected final concentration of AuroVist was 100 μg/cm^2 for preparation of cell batches 1 and 2, and 50 μg/cm^2 for preparation of batch 3, wherein <70% of the hMSC surface was covered by nanoparticles, and trypsin-induced gold hMSC detachment from the tissue culture plastic took <10 minutes. After 4 hours of incubation, a volume of medium containing 20% FBS was added to the cells to reach a final concentration of 10% FBS in the culture. Cells were incubated for an additional 20 hours, and then washed with phosphate-buffered saline (PBS). To remove GNPs from the cell surface, trypsin was added for 1–2 minutes and the flasks were rocked gently by hand to monitor cell detachment. When free GNPs were released from cell surface into the culture medium but cells were still attached to the plastic, the supernatant was collected and discarded. Additional trypsin was added for 6–10 minutes and the cells were harvested. Gold hMSCs were washed twice in PBS and filtered through 35-μm cell strainers. Neutron activation analysis was used to evaluate loading efficiency of hMSC batches with AuroVist as described in the following section.

Cell Migration Assay

Gold hMSCs were prepared as described in the previous section. Further, 50,000 gold hMSCs were transferred onto a Transwell (Corning, Sigma-Aldrich, St. Louis, MO) insert with 8-μm pores, and the insert was placed into a 24-well plate containing 0.5-mL Dulbecco modified eagle medium with 30% FBS and 4mM GlutaMAX. The same procedure was done with unmodified hMSCs (hMSC control). The cells were cultured overnight in a tissue culture incubator (at 37°C, 5% CO_2). After overnight culture, cells were removed from the upper side of the insert (nonmigrated cells). Cells that had migrated to the lower side of the insert were stained for 15–20 minutes with 0.2% gentian violet (in 4% paraformaldehyde). The inserts were washed and residual cells were removed from the upper side of the filter. The filters were placed onto a 24-well plate prepared with 0.5-mL PBS per well, and the migrated cells were analyzed with light microscopy at 10× magnification.

Neutron Activation Assay

Gold hMSCs and AuroVist standard samples were transferred to BioPal sample tubes and the suspensions were dried at 37°C. Standard samples were prepared with 1-μg/μL solution of AuroVist used for cell batch preparation. The gold content of each batch of gold hMSCs (3 batches) was analyzed. Standard neutron activation assays were performed by BioPhysics Assay Laboratory Inc. (BioPal, Worcester, MA).

Cell Lines and Tumor Models

Human breast cancer MDA-MB-231 cells were cultured in RPMI 1640 medium containing 10% FBS and 1% penicillin-streptomycin. Cells were cultured to up to 95% confluence, detached using trypsin, and suspended in Hank buffered saline solution for injection into mice. Female NOD-SCID mice were subcutaneously injected with 2 million cells on the upper right flank. At 2–3 weeks postinoculation, the tumors reached an average volume of 150 mm^3, whereupon the mice were divided into 3 groups, each containing 4 mice as follows: group 1: control (saline only), group 2: irradiated test group (saline + IR), and group 3: gold hMSC treatment + IR.

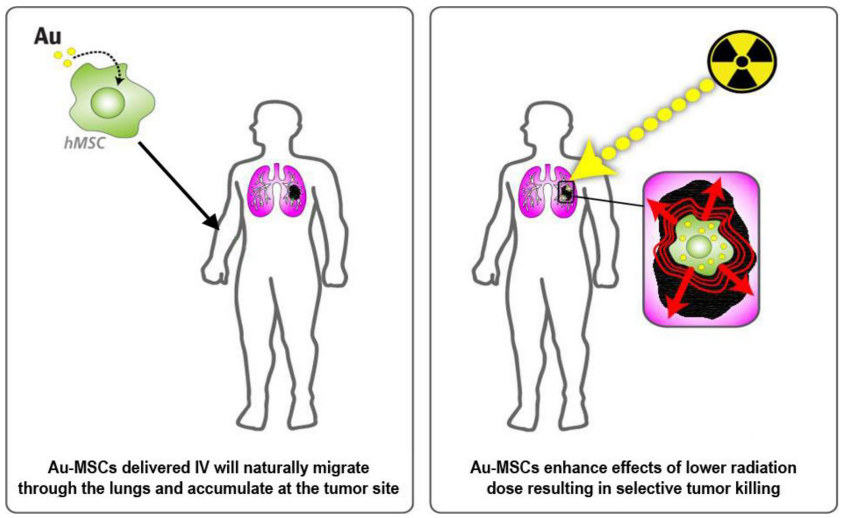

Figure 1. Concept of gold delivery for enhancement of radiotherapy.

Computed Tomography Imaging

Animal experiments were conducted in accordance with the policies of the Johns Hopkins Animal Care and Use Committee (ACUC). Mice bearing MDA-MB-231 tumors from group 3 were imaged before injection of cells or nanoparticles. At each time point, a fresh batch of gold hMSCs was prepared. Following imaging at baseline, mice were injected intravenously with an average of $(1.7 \pm 0.5) \times 10^6$ gold hMSCs on days 0, 3, and 6 for a total of 3 injections administered 72 hours apart. For imaging, mice were anesthetized with 3%isoflurane and maintained under 1.5% isoflurane. To follow gold hMSC accumulation at the tumor site, computed tomography (CT) images were acquired on a dedicated small-animal single-photon emission CT/CT (SPECT/CT) system (X-SPECT/CT, Gamma Medica Ideas, Northridge, CA) as 512 projections with a radius of rotation of 4 and a magnification of 3 at 72 hours after each injection of gold hMSCs. A total of 3 CT acquisitions were obtained per mouse. Images were reconstructed using the manufacturer's software and displayed and analyzed using AMIDE Medical Imaging Data Examiner (http://amide/sourceforge.net).

Radiotherapy

On day 8, 2 days after injection of gold hMSCs had been completed, mice were irradiated with the small animal radiation research platform (SARRP) as described previously (32). CT imaging was used for image-guided localization of the tumor. Mice from groups 2 and 3 were anesthetized with ketamine and irradiated with 220 kVp x-rays through a copper filter for a total dose of 30 Gy over a time interval of 16 minutes. Mice from group 1 were not irradiated, and these served as controls.

Tumor Measurements

Tumor growth was monitored by measurements that were manually recorded with a Vernier caliper 3 times per week. Weight of the mice was measured concurrently. Tumor volume was calculated using the modified ellipsoid formula $(l \times w^2)/2$. Tumor

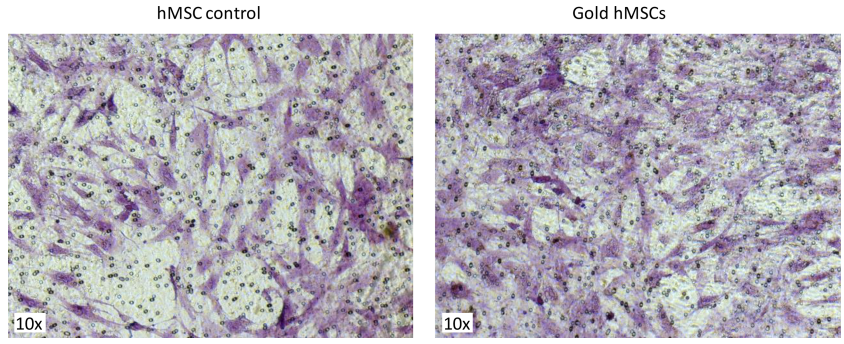

Figure 2. Cell migration assay. Unmodified control human mesenchymal stem cell (hMSCs) (left image) and gold nanoparticle-loaded hMSCs (right image) were transferred to Transwell inserts (8-μm pores), and the inserts were placed into a 24-well plate with chemoattractant stimuli. Cells that had migrated toward the chemoattractant stimuli were stained with 0.2% gentian violet solution and analyzed with light microscopy. Gold hMSCs show migratory potential comparable to unmodified, control hMSCs.

Figure 3. Computed tomography (CT) images of mice bearing MDA-MB-231 tumors 72 hours after each intravenous injection of gold hMSCs. The blue circle denotes tumor. Red dots within the blue circle show accumulation of high-density particles at the tumor site. Accumulation of gold hMSCs in the liver and spleen can be seen inferior to the diaphragm (white arrows).

measurements were recorded until the maximum tumor volume was 2,000 mm^3 or when there were visible signs of discomfort in the mice, whichever was earlier.

Statistical Analysis

Nonparametric Mann–Whitney test was selected for comparison of tumors among the groups of mice, given the small sample sizes (n = 4 in each group).

RESULTS

Preparation and Characterization of Gold hMSCs

A drawback of small GNPs is their low uptake into mammalian cells. To facilitate GNP uptake into hMSCs, protamine sulfate salt was added during incubation of cells with GNPs. Protamine sulfate is an FDA-approved polycationic peptide that has been used for gene transfection of cells and for the efficient labeling of MSCs with iron oxide (33). Protamine sulfate resulted in efficient uptake of GNPs with a diameter of 1.9 nm into the cytoplasm of hMSCs, which was confirmed using light microscopy. There was no reduction in cell viability, as evidenced by testing with trypan blue (data not shown). Gold hMSCs remained viable when kept in culture for up to 2 weeks. Those results confirm that the GNPs used in this study had no cytotoxic effect on the hMSCs. The ability to migrate toward chemoattractant stimuli is a prerequisite for gold hMSCs to reach a tumor site. The migratory potential of gold hMSCs was tested in chemotaxis Transwell assays, with 30% FBS as a chemoattractant. Figure 2 shows cells that had migrated through the pores of the Transwell insert toward the chemoattractant. Gold hMSCs (Figure 2, right) did not show signs of reduced migratory potential compared with unmodified control hMSCs (Figure 2, left). Neutron activation analysis of gold hMSCs revealed that the mice received an average amount of 4.6-mg gold per injection (4.3 mg first injection, 4.9 mg second injection, and 4.7 mg third injection).

CT Imaging and Radiotherapy

Before enhancement of radiotherapy, CT was performed in normal mice, with injection of GNPs alone in 2 doses (1 mg and

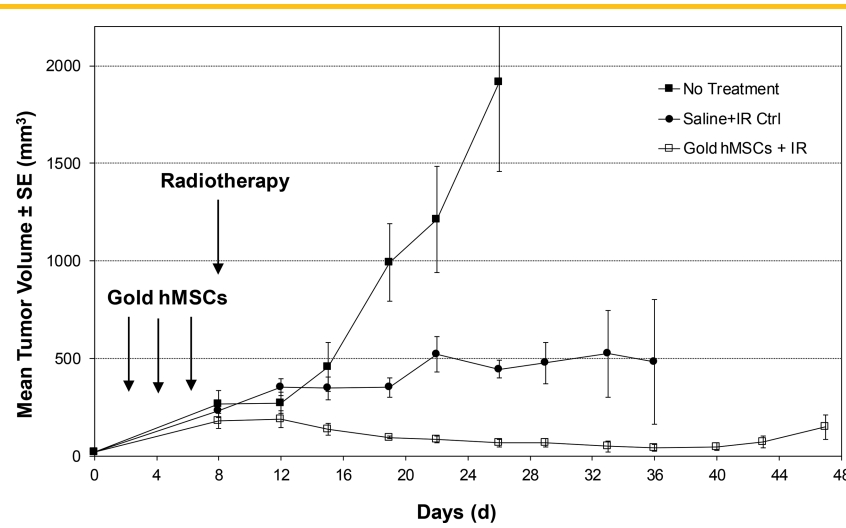

Figure 4. Enhanced radiotherapy of non-obese diabetic-severe combined immunodeficiency (NOD/SCID) mice harboring subcutaneous MDA-MB-231 tumor. Mice in group 1 received vehicle only, those in group 2 received vehicle plus irradiation (IR), and those in group 3 received gold hMSCs on 3 separate occasions before IR. In total, 4 animals were studied per group.

Table 1. Volume Changes in Tumor Growth

Saline + IR (%)	Gold hMSC + IR (%)
35.17	−56.93
162.53	−36.89
96.52	−79.10
84.07	−83.21

20 mg) to ascertain the minimum dose of nanoparticles needed to visualize contrast on CT. CT contrast was clearly visible in the bladder from 3 minutes up to 1 hour postinjection of GNPs at both doses (data not shown). Contrast was greater at a higher dose. Contrast was visible in the kidneys at 3 minutes and 5 minutes postinjection of the 20-mg dose. At the 1-hour imaging time point, GNPs were cleared from the kidneys. Gold hMSCs, on the other hand, demonstrated accumulation at the tumor site at 72 hours postinjection, which increased progressively after successive injections of the gold hMSCs (Figure 3). No discernible contrast was visible in the lungs, although the gold hMSCs do accumulate in other organs such as the liver and spleen (Figure 3). No acute toxicity was observed after injection of gold hMSCs.

Effect of Gold hMSCs Combined with Radiotherapy on Tumor Growth

Mice in group 1 (no treatment) reached a mean tumor volume of 2,000 mm^3 around day 24 following tumor inoculation (Figure 4). At that point, all mice in group 1 were euthanized as per guidelines of the Johns Hopkins ACUC. Mice from group 2 (saline + IR) exhibited delayed tumor growth, with mean tumor volumes being ∼500 mm^3 by day 36. Mice from group 3 (gold hMSCs + IR) exhibited the greatest delay in tumor growth, with a mean tumor volume of only 15 mm^3 at day 45 after tumor inoculation (Figure 4).

To compare the effects of radiation treatment with and without gold hMSCs quantitatively, we performed the Mann–Whitney test on the percent changes (%Vol) of tumor volumes, between the onset of treatment (day 8) and 18 days posttreatment (day 26). The %Vol values are shown in Table 1, and a statistically significant difference ($P = .0286$) was found, even with the small sample size available (n = 4 per group). The results indicate superior tumor control with the presence of GNPs homing to tumor compared with tumors that received standard IR alone.

DISCUSSION

We report potentiation of the effects of radiation therapy by gold hMSCs in tumors derived from a breast cancer cell line. Importantly, the GNPs could be efficiently loaded into the hMSCs with the use of protamine sulfate, and the addition of GNPs did not affect the ability of the hMSCs to migrate and home to tumors. That suggests that the methods reported here may represent a robust and generalizable method to target tumors with GNPs in order to improve the effectiveness of, as well as diminish the toxic effects of, externally applied radiation therapy.

Through CT, gold hMSC uptake in the tumors provided visual evidence compatible with the hypothesis that tumors behave like sites of injury in recruiting such cells. That property of the tumor microenvironment appears to facilitate an effective targeting mechanism to deliver drugs and other therapeutics to malignant tissues.

Previously, Hainfeld et al. reported enhancement of radiotherapy in tumor-bearing mice after intravenous injection of GNPs without hMSCs as a carrier. In that instance, without such a delivery vehicle for GNPs, mice required radiotherapy at 2 minutes postinjection of the GNPs to avoid lowering of GNP concentration at the tumor site, that is, washout, before treatment (29). In our study, gold hMSC accumulation at the tumor site was detected at later time points and allowed for treatment with radiotherapy at 72 hours after the last injection of gold hMSCs, which might portend a clinically feasible protocol. The difference between GNP biodistribution after IV injection of free GNPs (29) and gold hMSCs indicates that GNPs in our study were not released before arrival at the tumor site, and that hMSCs functioned as an effective delivery tool for the GNPs. The unique ability of MSCs to migrate to sites of inflammation and cancer together with their low immunogenicity make them an attractive delivery vehicle for the treatment of diseases with inflammatory components. The accumulated data indicate that after systemic delivery, MSCs do not engraft (34). The majority of MSCs do not survive after infusion, and MSCs appear to mediate their therapeutic effect via a paracrine mechanism. The lack of MSC-sustained engraftment is a positive outcome that limits the potential long-term risks of MSC therapy.

Limitations of the current work include the small sample size (4 mice per group) and the single type of tumor studied (MDA-MB-231 breast cancer cell line–derived tumors). Furthermore, in this study, we did not specifically address potential effects of gold hMSCs on normal tissues and whether there may be enhanced toxicity; further work will be needed to address this important consideration. Nevertheless, the results presented show a statistically significant contribution of gold hMSCs to the antitumor effects of radiation therapy in the studied context. That finding merits further evaluation across a broader array of tumor types to confirm this effect and lay the groundwork for potential clinical translation.

CONCLUSION

We report the development of GNP-loaded hMSCs (gold hMSCs) and their successful use for enhancement of radiation therapy in mice bearing tumors derived from a breast cancer cell line. Gold hMSCs retained their ability to migrate, an essential property for cell use as a drug delivery vehicle. Intravenous injection of gold hMSCs was well-tolerated, with no acute toxicity observed in the treated animals. Repeated injection of gold hMSCs resulted in the accumulation of GNPs at the tumor site and enhanced the effect of radiotherapy. Other permutations of the gold hMSCs/IR treatment may achieve complete eradication of tumor.

ACKNOWLEDGMENT

We thank CA151838, EB024495, and OSIRIS Therapeutics for financial support, and Dr. John Wong and Esteban Velarde of SARRP at Johns Hopkins University for help with irradiation.

REFERENCES

1. Delaney G, Jacob S, Featherstone C, Barton M. The role of radiotherapy in cancer treatment: estimating optimal utilization from a review of evidence-based clinical guidelines. Cancer. 2005;104:1129–1137.
2. Barnett GC, West CM, Dunning AM, Elliott RM, Coles CE, Pharoah PD, Burnet NG. Normal tissue reactions to radiotherapy: towards tailoring treatment dose by genotype. Nat Rev Cancer. 2009;9:134–142.
3. Wardman P. Chemical radiosensitizers for use in radiotherapy. Clin Oncol (R Coll Radiol). 2007;19:397–417.
4. Naylor MA, Thomson P. Recent advances in bioreductive drug targeting. Mini Rev Med Chem. 2001;1:17–29.
5. Wardman P. Electron transfer and oxidative stress as key factors in the design of drugs selectively active in hypoxia. Curr Med Chem. 2001;8:739–761.
6. Raleigh DR, Haas-Kogan DA. Molecular targets and mechanisms of radiosensitization using DNA damage response pathways. Future Oncology. 2013;9:219–233.
7. Butterworth KT, Coulter JA, Jain S, Forker J, McMahon SJ, Schettino G, Prise KM, Currell FJ, Hirst DG. Evaluation of cytotoxicity and radiation enhancement using 1.9 nm gold particles: potential application for cancer therapy. Nanotechnology. 2010;21:295101.
8. Scientific basis for the definition of "nanomaterial". http://ec.europa.eu/health/scientific_committees/emerging/docs/scenihr_o_032.pdf. Accessed on March 26, 2020.
9. Gerber A, Bundschuh M, Klingelhofer D, Groneberg DA. Gold nanoparticles: recent aspects for human toxicology. J Occup Med Toxicol. 2013;8:32.
10. Hainfeld JF, Dilmanian FA, Slatkin DN, Smilowitz HM. Radiotherapy enhancement with gold nanoparticles. J Pharm Pharmacol. 2008;60:977–985.
11. Rahman WN, Bishara N, Ackerly T, He CF, Jackson P, Wong C, Davidson R, Geso M. Enhancement of radiation effects by gold nanoparticles for superficial radiation therapy. Nanomedicine. 2009;5:136–142.
12. Choi HS, Liu W, Misra P, Tanaka E, Zimmer JP, Itty Ipe B, Bawendi MG, Frangioni JV. Renal clearance of quantum dots. Nat Biotechnol. 2007;25:1165–1170.
13. Zhang XD, Yang J, Song SS, Long W, Chen J, Shen X, Wang H, Sun YM, Liu PX, Fan S. Passing through the renal clearance barrier: toward ultrasmall sizes with stable ligands for potential clinical applications. Int J Nanomedicine. 2014;9:2069–2072.
14. Jiang J, Chen W, Zhuang R, Song T, Li P. The effect of endostatin mediated by human mesenchymal stem cells on ovarian cancer cells in vitro. J Cancer Res Clin Oncol. 2010;136:873–881.
15. Khakoo AY, Pati S, Anderson SA, Reid W, Elshal MF, Rovira II, Nguyen AT, Malide D, Combs CA, Hall G, Zhang J, Raffeld M, Rogers TB, Stetler-Stevenson W, Frank JA, Reitz M, Finkel T. Human mesenchymal stem cells exert potent antitumorigenic effects in a model of Kaposi's sarcoma. J Exp Med. 2006;203:1235–1247.
16. Loebinger MR, Eddaoudi A, Davies D, Janes SM. Mesenchymal stem cell delivery of TRAIL can eliminate metastatic cancer. Cancer Res. 2009;69:4134–4142.
17. Xin H, Kanehira M, Mizuguchi H, Hayakawa T, Kikuchi T, Nukiwa T, Saijo Y. Targeted delivery of CX3CL1 to multiple lung tumors by mesenchymal stem cells. Stem Cells. 2007;25:1618–1626.
18. Studeny M, Marini FC, Champlin RE, Zompetta C, Fidler IJ, Andreeff M. Bone marrow-derived mesenchymal stem cells as vehicles for interferon-beta delivery into tumors. Cancer Res. 2002;62:3603–3608.
19. Spaeth E, Klopp A, Dembinski J, Andreeff M, Marini F. Inflammation and tumor microenvironments: defining the migratory itinerary of mesenchymal stem cells. Gene Ther. 2008;15:730–738.
20. Kim SM, Jeong CH, Woo JS, Ryu CH, Lee JH, Jeun SS. In vivo near-infrared imaging for the tracking of systemically delivered mesenchymal stem cells: tropism for brain tumors and biodistribution. Int J Nanomedicine. 2015;11:13–23.
21. Layek B, Sadhukha T, Panyam J, Prabha S. Nano-engineered mesenchymal stem cells increase therapeutic efficacy of anticancer drug through true active tumor targeting. Mol Cancer Ther. 2018;17:1196–1206.
22. Serakinci N, Cagsin H. Programming hMSCs into potential genetic therapy in cancer. Crit Rev Eukaryot Gene Expr. 2019;29:343–350.
23. Putz Todd G, LeRoux MA, Danilkovitch-Miagkova A. Mesenchymal stem cells as vehicles for targeted therapies. In: Drug Discovery and Development – Present and Future. Ed. Kapetanovic IM. IntechOpen.
24. Arnida MA, Ghandehari H. Cellular uptake and toxicity of gold nanoparticles in prostate cancer cells: a comparative study of rods and spheres. J Appl Toxicol. 2010;30:212–217.
25. Chithrani BD, Chan WC. Elucidating the mechanism of cellular uptake and removal of protein-coated gold nanoparticles of different sizes and shapes. Nano Lett. 2007;7:1542–1550.
26. Yamada S, Fujita S, Uchimura E, Miyake M, Miyake J. Reverse transfection using gold nanoparticles. Methods Mol Biol. 2009;544:609–616.
27. Chithrani BD, Ghazani AA, Chan WC. Determining the size and shape dependence of gold nanoparticle uptake into mammalian cells. Nano Lett. 2006;6:662–668.
28. Arnida Janát-Amsbury MM, Ray A, Peterson CM, Ghandehari H. Geometry and surface characteristics of gold nanoparticles influence their biodistribution and uptake by macrophages. Eur J Pharm Biopharm. 2011;77:417–423.
29. Hainfeld JF, Slatkin DN, Smilowitz HM. The use of gold nanoparticles to enhance radiotherapy in mice. Phys Med Biol. 2004;49:N309–N315.
30. Hainfeld JF, Slatkin DN, Focella TM, Smilowitz HM. Gold nanoparticles: a new X-ray contrast agent. Br J Radiol. 2006;79:248–253.
31. Kebriaei P, Isola L, Bahceci E, Holland K, Rowley S, McGuirk J, Devetten M, Jansen J, Herzig R, Schuster M, Monroy R, Uberti J. Adult mesenchymal stem cells added to corticosteroid therapy for the treatment of acute graft-versus-host disease. Biol Blood Marrow Transplant. 2009;15:804–811.
32. Wong J, Armour E, Kazanzides P, Iordachita I, Tryggestad E, Deng H, Matinfar M, Kennedy C, Liu Z, Chan T, Gray O, Verhaegen F, McNutt T, Ford E, DeWeese TL. High-resolution, small animal radiation research platform with x-ray tomographic guidance capabilities. Int J Radiat Oncol Biol Phys. 2008;71:1591–1599.
33. Arbab AS, Yocum GT, Kalish H, Jordan EK, Anderson SA, Khakoo AY, Read EJ, Frank JA. Efficient magnetic cell labeling with protamine sulfate complexed to ferumoxides for cellular MRI. Blood. 2004;104:1217–1223.
34. von Bahr L, Batsis I, Moll G, Hägg M, Szakos A, Sundberg B, Uzunel M, Ringden O, Le Blanc K. Analysis of tissues following mesenchymal stromal cell therapy in humans indicates limited long-term engraftment and no ectopic tissue formation. Stem Cells. 2012;30:1575–1578.